BIOCHEMISTRY
including biophysical chemistry & molecular biology
Article

Biochemistry **2010,** *49,* 7879–7891 7879
DOI: 10.1021/bi100889r

Nonspecific DNA Binding and Coordination of the First Two Steps of Base Excision Repair[†]

Michael R. Baldwin and Patrick J. O'Brien*

Department of Biological Chemistry, University of Michigan, Ann Arbor, Michigan 48109

Received June 2, 2010; Revised Manuscript Received August 2, 2010

ABSTRACT: The base excision repair (BER) pathway repairs a wide variety of damaged nucleobases in DNA. This pathway is initiated by a DNA repair glycosylase, which locates the site of damage and catalyzes the excision of the damaged nucleobase. The resulting abasic site is further processed by apurinic/apyrimidinic site endonuclease 1 (APE1) to create a single-strand nick with the 3′-hydroxyl that serves as a primer for DNA repair synthesis. Because an abasic site is highly mutagenic, it is critical that the steps of the BER pathway be coordinated. Most human glycosylases bind tightly to their abasic product. APE1 displaces the bound glycosylase, thereby stimulating multiple-turnover base excision. It has been proposed that direct protein−protein interactions are involved in the stimulation by APE1, but no common interaction motifs have been identified among the glycosylases that are stimulated by APE1. We characterized the APE1 stimulation of alkyladenine DNA glycosylase (AAG) using a variety of symmetric and asymmetric lesion-containing oligonucleotides. Efficient stimulation of a wide variety of substrates favors a model in which both AAG and APE1 can simultaneously bind to DNA but may not interact directly. Rather, nonspecific DNA binding by both AAG and APE1 enables APE1 to replace AAG at the abasic site. AAG is not displaced into solution but remains bound to an adjacent undamaged site. We propose that nonspecific DNA binding interactions allow transient exposure of the abasic site so that it can be captured by APE1.

The base excision repair (BER)[1] pathway repairs a wide variety of damaged nucleobases in DNA. There are at least 11 human DNA repair glycosylases that locate damaged nucleotides, and these enzymes initiate the BER pathway by catalyzing the hydrolysis of the *N*-glycosidic bond to release the base lesion. Although several of these enzymes have associated lyase activity that can cleave the DNA backbone, most of the human glycosylases create an abasic DNA product. The major abasic site-specific endonuclease, AP endonuclease I (APE1), is responsible for hydrolyzing the abasic site and creating a 3′-hydroxyl and a 5′-deoxyribose phosphate end. Subsequently, polymerase β incorporates the correct nucleotide with its DNA polymerase active site and removes the deoxyribose phosphate group with its lyase active site. DNA ligase seals the nick to complete the repair pathway.

Most DNA glycosylases bind tightly to the abasic DNA product, and this provides a mechanism for protecting the abasic site and coordinating the catalytic action of the glycosylase and APE1 (*1*−*7*). In several cases, APE1 has been shown to increase the rate of dissociation of the glycosylase (*2*, *6*−*8*). It has been suggested that this stimulated rate of dissociation involves direct protein−protein interactions; however, the exact nature of this interaction has not been resolved for any glycosylase (*2*, *6*, *7*). We have addressed the question of how the BER pathway is coordinated with human alkyladenine DNA glycosylase (AAG). AAG is responsible for repairing a wide variety of alkylated and deaminated purine lesions (*9*, *10*). One of the most efficient substrates for AAG is deoxyinosine (I), which is formed from the oxidative deamination of deoxyadenosine (*11*, *12*). AAG-catalyzed hydrolysis of I yields the abasic-containing DNA and the free base hypoxanthine (Hx). We previously reported kinetic experiments establishing that multiple turnovers of AAG on I·T substrates are limited by the rate of dissociation from the abasic DNA product and that APE1 stimulates turnover by increasing this rate (*8*). This finding is consistent with the model in which APE1 stimulates AAG via direct physical interaction, as has been previously proposed for AAG and for other DNA glycosylases (*6*, *7*, *13*). However, the nature of a possible APE1−AAG interaction is unknown. Therefore, we have tested this hypothesis by comparing the kinetics for APE1 stimulation of AAG with a series of substrates that differ in the size of the nonspecific DNA flanking the site of damage. If APE1 and AAG were to form a specific complex, even transiently, then this complex would involve additional DNA interactions beyond those required for AAG alone. A previous report used this strategy to conclude that APE1 preferentially interacts with 8-oxoguanine DNA glycosylase (OGG1) on the 5′ side of the site of damage (*7*).

All of the BER enzymes are expected to have a reasonably high affinity for undamaged DNA, and nonspecific DNA binding is presumed to play an important role in locating sites of damage. Both AAG (*14*) and APE1 (*15*) have been shown to use nonspecific DNA binding interactions to locate sites of damage via a processive searching mechanism. These processivity assays

[†]This work was supported by a grant from the National Institutes of Health to P.J.O. (CA122254).

*To whom correspondence should be addressed. Phone: (734) 647-5821. Fax: (734) 764-3509. E-mail: pjobrien@umich.edu.

[1]Abbreviations: AAG, alkyladenine DNA glycosylase, also known as methylpurine DNA glycosylase (MPG) and 3-methyladenine DNA glycosylase; AP, apurinic/apyrimidinic site; APE1, AP endonuclease I, also known as APEX1; BER, base excision repair; BSA, bovine serum albumin; DTT, dithiothreitol; EDTA, ethylenediaminetetraacetate; EndoIII, endonuclease III encoded by the *Nth* gene; Hx, hypoxanthine (base moiety of inosine); I, deoxyinosine; NaHEPES, sodium *N*-(2-hydroxyethyl)piperazine-*N*′-2-ethanesulfonate; NaMES, sodium 2-(*N*-morpholino)ethanesulfonate; OGG1, 8-oxoguanine DNA glycosylase; PAGE, polyacrylamide gel electrophoresis; PEG, polyethylene glycol.

Published on Web 08/11/2010

directly show that AAG can leave an abasic site and locate another site of damage located on the same DNA molecule. Transient excursions of AAG away from the abasic site would provide an opportunity for another enzyme, such as APE1, to translocate from an adjacent nonspecific site onto the abasic site. Such a mechanism would not require protein−protein interactions and would be a general mechanism by which proteins could attain the most thermodynamically favorable complexes without dissociation into solution.

We investigated the mechanism by which APE1 accelerates the rate of dissociation of AAG from its abasic DNA product by systematically comparing the kinetic parameters for glycosylase activity on a series of homologous substrates that differ in the amount of nonspecific DNA available. The results suggest that APE1 can efficiently displace AAG from either upstream or downstream of the abasic site with as little as 6 bp of flanking DNA required. Robust stimulation of AAG dissociation is also observed for another enzyme that can compete for the abasic DNA product, *Escherichia coli* endonuclease III (EndoIII). These experiments demonstrate that an AAG-bound abasic site is transiently accessible to other DNA binding proteins and reveal a remarkably small footprint for the simultaneous binding of APE1 and AAG. There is now abundant evidence that nonspecific DNA binding interactions are key not only to finding sites of damage but also to the transfer of repair intermediates between enzyme active sites in the BER pathway.

MATERIALS AND METHODS

Recombinant Proteins. Full-length human APE1 was purified as previously described (*8*). Full-length human AAG was cloned into an *E. coli* expression vector that contained an N-terminal six-His SUMO tag and verified by sequencing the open reading frame. This expression vector (termed ppSUMO) was a gift from P. Pellicini and was originally derived from pET28 (Novagen), with the open reading frame for yeast smt3 inserted between the NcoI and BamHI sites. The open reading frame for full-length AAG was PCR-amplified, digested with BamHI and XhoI, and ligated into the ppSUMO vector that had been cut by the same enzymes. The desired construct was verified by sequencing the entire open reading frame of the SUMO fusion. This new expression construct greatly increased the yields of the full-length protein. The purification of the SUMO fusion was essentially identical to the previous purification of the 10-His-tagged full-length AAG (*16*), except that removal of the tag was achieved via treatment with the SUMO isopeptidase ULP1 after the metal affinity column and prior to the anion exchange step. The resulting protein differs by two amino acids at the amino terminus and had glycosylase activity identical to that of the previously characterized protein (data not shown). Full-length *E. coli* EndoIII was cloned using primers that were designed to anneal to the upstream and downstream ends of the Nth (EndoIII) open reading frame. The appropriate fragment was PCR amplified from DH5α genomic DNA and digested with BamHI and XhoI using sites that were engineered into the PCR primers. This fragment was cloned into ppSUMO, which had been digested with the same restriction enzymes. The open reading frame was sequenced and found to be identical to the genomic sequence for Nth from the *E. coli* K12 genome. The SUMO fusion was expressed in BL21(DE3) at 37 °C, and cells were lysed in 50 mM KP_i (pH 7.4), 200 mM NaCl, 10% glycerol, and 5 mM β-mercaptoethanol. After an initial purification on a Ni^{2+}-NTA column, the SUMO tag was removed with ULP1, and the protein was further purified on heparin sulfate. Peak fractions were pooled and concentrated to ~4 mg/mL and stored at −80 °C. The concentration was determined from the absorbance at 280 nm, using a calculated extinction coefficient (E_{280}) of 1.85×10^4 M^{-1} cm^{-1}. The purity was estimated to be ≥95% based upon SDS−PAGE analysis using Coomassie staining.

Oligonucleotides. DNA substrates were synthesized by Integrated DNA Technologies or the Keck Center at Yale University (New Haven, CT) and were purified by denaturing PAGE as previously described (*8*). The concentration of single-stranded DNA was determined from the absorbance at 260 nm using the calculated extinction coefficients, and the concentration of duplex (hairpin) DNA was determined from the extinction coefficient at 495 nm for fluorescein ($E_{495} = 7.5 \times 10^5$ M^{-1} cm^{-1}). In all cases, a more precise measure of the DNA concentration was determined by burst analysis, assuming a stoichiometric burst of Hx release by AAG. These corrections were less than 30% in all cases.

General Glycosylase Activity Assay. DNA substrates were labeled on the lesion-containing strand with 5′-fluorescein and were assayed as previously described (*8*). All assays were conducted at 37 °C. Unless otherwise indicated, the reaction conditions included 50 mM NaHEPES (pH 7.0), 1 mM EDTA, 1 mM DTT, 10% (v/v) glycerol, 0.1 mg/mL BSA, and sufficient NaCl to reach an ionic strength of 42 mM. Reaction volumes ranged from 15 to 30 μL, depending on the number of time points to be taken. At the desired times, aliquots were withdrawn and quenched by mixing with 2 volumes of 0.3 M NaOH to attain a final concentration of 0.2 M NaOH. Abasic sites were quantitatively converted into DNA breaks by heating for 15 min at 70 °C. Samples were mixed with 3.3 volumes of formamide/EDTA loading buffer, heated for 2 min at 70 °C, and analyzed on denaturing polyacrylamide sequencing gels (10 to 20%) containing saturating urea (6−8 M). Gels were scanned with a typhoon trio imager using 488 nm excitation and a 520 nm long pass filter to detect fluorescein. Intensities of product and substrate bands were quantified using Image Quant TL (GE Healthcare), and the fraction product at each time point was calculated according to eq 1

$$F = P/(P+S) \quad (1)$$

where F is the fraction of substrate converted to product, P is the amount of product, and S is the amount of intact substrate. Reaction progress curves were analyzed using Kaleidagraph (Synergy Software), as described below.

Single-Turnover Glycosylase Assay. Single-turnover glycosylase assays were performed in the standard reaction buffer, as described above. Reactions were followed to completion (at least six half-lives), and the fraction product was fit by a single exponential using Kaleidagraph (eq 2).

$$\text{fraction product} = A[1 - \exp(-k_{obs}t)] \quad (2)$$

The concentration of AAG was in excess over the concentration of DNA substrate (typically 50 nM) to ensure single-turnover conditions. In all cases, the observed single-turnover rate constant was independent of the concentration of AAG, which was varied by at least 5-fold (see the Supporting Information). This observed rate constant corresponds to the saturating single-turnover rate constant ($k_{obs} = k_{max}$) and monitors steps after binding up to and including the chemical step (eq 3).

$$k_{obs} = k_{max}[AAG]/(K_{1/2} + [AAG]) \quad (3)$$

Multiple-Turnover Glycosylase Assay. Multiple-turnover AAG reactions in the presence and absence of APE1 were

performed as previously described (*8*). Typically, the concentration of substrate was 1 μM and the concentration of AAG was 25 nM. When APE1 was present it was at a concentration of 2 μM, safely in excess over the number of substrate molecules. We varied the concentration of APE1 to ensure that it was saturating, and identical stimulation was observed for APE1 concentrations between 1 and 4 μM (see the Supporting Information). After storage at 4 °C for several weeks, we noted that APE1 lost its ability to fully stimulate AAG (data not shown). We presume that this loss of activity is related to oxidation, because APE1 is known to be susceptible to oxidation (*17*), and incubation of APE1 that had lost its activity at 4 °C in fresh DTT at 37 °C resulted in a partial recovery of the ability of APE1 to stimulate AAG (data not shown). We routinely stored APE1 at −80 °C or in 50% glycerol at −20 °C. Regardless of the storage method, there was no detectable loss of activity for at least 6 months.

Initial rates were routinely determined from linear fits to time points taken before 20% substrate was consumed. At saturating substrate, the Michaelis−Menten equation (eq 4) simplifies to eq 5.

$$V_{obs} = k_{cat}[E][S]/(K_M + [S]) \quad (4)$$

$$V_{obs} = k_{cat}[E] \quad (5)$$

To examine the effects of product inhibition for APE1-stimulated AAG reactions, time courses were extended so that >85% of the substrate was consumed. Reactions that took place at different rates were compared visually by using a double *x*-axis, thereby allowing the curvature due to product inhibition to be directly compared. Simulations and curve fitting were performed with Berkeley Madonna (www.berkeleymadonna.com) to evaluate the relative affinities of AAG for intact substrates and APE1-bound products (see the Supporting Information).

In the absence of Mg^{2+}, a very slow endonuclease activity was observed after long incubation times, but the amount of hydrolysis that occurred during the initial rate portion of the AAG reaction was negligible (*8*, *18*). We observed that the hairpin connected by a PEG linker was susceptible to cleavage by APE1, even in the absence of Mg^{2+}, with strand nicking occurring immediately 5′ to the PEG (see the Supporting Information). This is consistent with the ability of APE1 to catalyze incision of DNA 5′ to helix-distorting moieties, such as α-anomeric nucleotides (*19*, *20*). In the presence of Mg^{2+}, the APE1-catalyzed incision was extremely fast (data not shown). Under the EDTA-buffered conditions that we employed for the multiple-turnover glycosylase assays, this additional reaction did not interfere with our measurements, because AAG excised the Hx lesion at least 10-fold more quickly than APE1 could nick at the PEG linker (see the Supporting Information). No endonuclease reaction was observed toward a hairpin linked with a GAAA tetraloop (data not shown).

Stimulation of AAG by *E. coli* EndoIII was assessed as described for APE1 above. Under these conditions, EndoIII was active as an AP lyase (data not shown). Control reactions in which AAG was omitted revealed a very slow rate of Hx excision and AP lyase activity consistent with an EndoIII-catalyzed glycosylase reaction with the inosine substrate. The activity of EndoIII toward inosine has not been previously reported, but EndoIII accepts a wide range of substrates; therefore, it is not surprising that some activity was observed (*21*, *22*). This AAG-independent reaction was negligible under the conditions employed and did not significantly affect the calculation of the stimulation (see the Supporting Information).

Determination of Relative k_{cat}/K_M Values. It was not practical to directly measure k_{cat} and K_M values for the AAG- and APE1-catalyzed reactions using the fluorescence-based assays, due to the extremely low K_M values. Therefore, we took advantage of the fact that the competition for two substrates (designated A and B) binding to a single active site gives velocities that are proportional to the k_{cat}/K_M values for the two substrates [eq 6 (*23*)]. Thus, we mixed together the two substrates to be compared and followed both reactions in a single reaction tube (see the Supporting Information for additional details and representative data).

$$V_A/V_B = [[A](k_{cat}/K_M)_A]/[[B](k_{cat}/K_M)_B] \quad (6)$$

RESULTS

APE1 stimulates the multiple-turnover glycosylase activity of AAG by increasing the rate of dissociation from its abasic DNA product (*8*). This stimulation does not require APE1 endonuclease activity, because full stimulation of AAG occurs in the absence of Mg^{2+}, which is required for maximal APE1 catalytic activity. To facilitate comparison with previously published results, and to minimize complications with APE1-catalyzed strand nicking, we have performed AAG reactions in the absence of Mg^{2+}. Under these conditions, APE1 binds with extremely high affinity to abasic sites and minimal strand nicking occurs (*24*, *25*). This allows us to focus on the first steps of BER, those that involve the binding, base excision, and release of the glycosylase. The stimulatory effect of APE1 is most pronounced at lower ionic strengths, because the dissociation of AAG is strongly influenced by ionic strength. Low ionic strength conditions have been used in this study (42 mM) to provide a large dynamic range for the stimulation of AAG; however, this stimulation is also observed at higher ionic strengths [120 mM (*8*)]. We have determined the kinetic parameters for the stimulation of AAG by APE1 for both symmetric and asymmetric oligonucleotides to gain insight into the mechanism by which APE1 displaces AAG from the abasic DNA product. Oligonucleotide substrates were designed to contain a single I·T lesion in an identical sequence context but to differ in the length and structure of the 5′ or 3′ flanking regions (Figure 1). It is important to maintain the same sequence context, because large differences in Hx excision rates have been attributed to differences in sequence context (*26*, *27*). To evaluate the possible requirement for flanking DNA on the displacement of AAG by APE1, we characterized the glycosylase activity toward each substrate and the rate of glycosylase release from each abasic product in the presence and absence of APE1.

A simplified kinetic mechanism for AAG-catalyzed base excision and the effect of APE1 has been adapted from previous work and is shown in Figure 2 (*8*). DNA binding by AAG occurs in two distinct steps, with initial DNA binding followed by nucleotide flipping to place the *N*-glycosidic bond in the enzyme active site (*28*, *29*). Under the saturating conditions employed, these steps are expected to be very rapid. Whereas the equilibrium constant for flipping of the alkylated lesion 1,N^6-etheno-dA is highly favorable (*28*), previous work suggests that the equilibrium constant for flipping of I is unfavorable (*9*, *30*). Therefore, the maximal single-turnover rate constant (k_{max}) reports on both this unfavorable equilibrium and the rate constant for *N*-glycosidic bond hydrolysis (*9*). Multiple turnovers are limited by the rate of dissociation from the abasic DNA product ($k_{cat} = k_{off}$), whereas the presence of saturating APE1 ensures that the dissociation step is no longer rate-limiting for multiple turnovers (i.e., $k_{cat}^{APE1} = k_{max}$).

```
49  5'-GACATGATTGCCCGATAGCATCCTICCTTCTCTCCATGCGTCAATTGTC(FAM)
    3'-CTGTACTAACGGGCTATCGTAGGATGGAAGAGAGGTACGCAGTTAACAG

35    5'-(FAM)TTGCCCGATAGCATCCTICCTTCTCTCCATGCGTC
            3'-AACGGGCTATCGTAGGATGGAAGAGAGGTACGCAG

25          5'-(FAM)CGATAGCATCCTICCTTCTCTCCAT
                  3'-GCTATCGTAGGATGGAAGAGAGGTA

21d         5'-(FAM)CGATAGCATCCTICCTTCTCT
                  3'-GCTATCGTAGGATGGAAGAGA

19d         5'-(FAM)CGATAGCATCCTICCTTCT
                  3'-GCTATCGTAGGATGGAAGA

HP19d       5'-(FAM)CGATAGCATCCTICCTTCTGA]
                  3'-GCTATCGTAGGATGGAAGAAA

19u               5'-(FAM)CATCCTICCTTCTCTCCAT
                        3'-GTAGGATGGAAGAGAGGTA

HP19u                   [AACATCCTICCTTCTCTCCAT-3'
                        AGGTAGGATGGAAGAGAGGTA(FAM)-5'

HP19uPEG              PEG[CATCCTICCTTCTCTCCAT-3'
                          GTAGGATGGAAGAGAGGTA(FAM)-5'

19             5'-(FAM)TAGCATCCTICCTTCTCTC
                     3'-ATCGTAGGATGGAAGAGAG

17              5'-(FAM)AGCATCCTICCTTCTCT-3'
                      3'-TCGTAGGATGGAAGAGA-5'

HP17PEG         5'-(FAM)AGCATCCTICCTTCTCT] PEG
                      3'-TCGTAGGATGGAAGAGA
```

FIGURE 1: DNA substrates used in this study. The local sequence context of the I·T mismatch was maintained in all cases. The position of the fluorescein (FAM) label is indicated. A normal phosphodiester bond connects the two strands for the GAAA tetraloop hairpin substrates (HP), whereas in the polyethylene glycol (PEG) hairpins, the two strands are bridged by six ethylene glycol units.

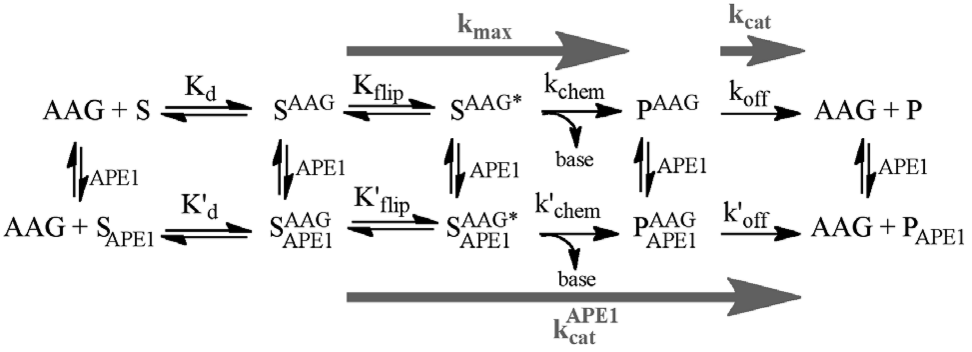

FIGURE 2: Kinetic mechanism for AAG-catalyzed base excision and stimulation by APE1. The DNA substrate is abbreviated S and the abasic DNA product P. Gray arrows are used to indicate the steps that are monitored by multiple-turnover (k_{cat}) or single-turnover (k_{max}) kinetics. APE1 selectively increases the rate of AAG dissociation (k'_{off}), without affecting other steps in the AAG reaction (e.g., $k_{chem} = k'_{chem}$).

Single-Turnover Glycosylase Activity of AAG toward Inosine Lesions Located Different Distances from the DNA Ends. Oligonucleotides with a central I·T mismatch as short as 17 bp are very good substrates of AAG, and the *N*-glycosidic bond cleavage measured by a single-turnover reaction is only 50% lower for a 17mer substrate than for a 25mer substrate (*8*). We wanted to confirm that the 25mer substrate, with 12 bp of flanking DNA on each side, fully satisfied the binding requirements of AAG. Therefore, we measured single-turnover excision of Hx from 35- and 49mer symmetric substrates (Figure 1). The glycosylase reactions followed a single exponential in all cases, and the rate constants were independent of the concentration of AAG, confirming that the saturating single-turnover rate constant was determined (see Materials and Methods for details). Representative data are shown in Figure 3A, and the rate constants are listed in Table 1. These longer substrates behaved very much like the previously characterized 25mer (*8*). The observation that the single-turnover rate constant is essentially identical for symmetric substrates with 12−24 bp of flanking DNA indicates that all of the AAG−DNA contacts occur within 12 bp upstream and downstream of the lesion site.

We next compared the rates of single-turnover excision of Hx from two asymmetric substrates that were based upon the 25mer sequence but were shortened to 6 bp on either the 5′ (19u) or 3′ (19d) side of the lesion (Figure 1). Both substrates were rapidly hydrolyzed under single-turnover conditions, indicating that they are good substrates for AAG (Figure 3B). Shortening of the 5′ side is fully tolerated, but shortening of the 3′ side results in a

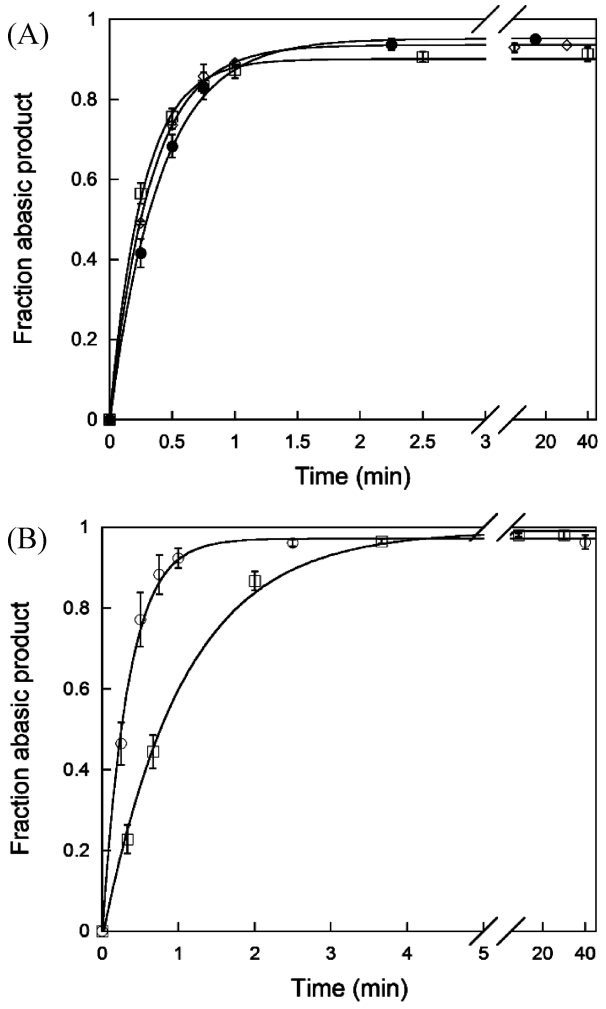

FIGURE 3: Single-turnover excision of Hx by AAG. Representative data for select substrates are shown. (A) The results for the symmetric 35mer (□) and 49mer (◇) sequences are compared to previously published results for the 25mer (●) sequence (*8*). (B) Results for asymmetric substrates that were shortened at either the upstream (19u, ○) or downstream (19d, □) flanking region. The average of two or three independent reactions is shown, and the error bars indicate the standard deviations.

modest ~2-fold reduction of the single-turnover base excision rate (k_{max}) relative to that of the 25mer (Table 1). We also tested an asymmetric substrate that maintained the same 12 bp upstream, but with 8 bp on the downstream side [21d (Figure 1)]. The addition of 2 bp to the downstream flanking region led to a 2-fold increase in the k_{max} value (Table 1). Increasing the DNA length on the downstream side to 12 bp has only an additional 1.4-fold effect [25mer (Table 1)]. These data indicate that the 6 bp flanking regions are sufficient for robust AAG activity and suggest that they are appropriate substrates for investigating the stimulation of AAG by APE1.

Multiple-Turnover Excision of Hx by AAG and Stimulation by APE1. We used multiple-turnover kinetics to gain insight into the AAG product release step and the effect of APE1 on this step. By comparing the k_{cat} values for excision of Hx from substrates with different lesion positions, we expected to identify the minimal site size required by AAG for binding to an abasic DNA. This is because k_{cat} is limited by the rate of dissociation from the abasic DNA product (*8*). A decreased k_{cat} value indicates that AAG dissociates more slowly from its abasic product (i.e., binds more tightly), relative to a substrate with an increased k_{cat} value. This analysis requires that the same kinetic mechanism apply for all of the substrates. Therefore, we performed burst experiments to confirm that the product release step is rate-limiting for substrates in which the lesion site is closer to the end. In all cases, the expected burst was observed (ref *8* and data not shown). These burst experiments also provided an accurate determination of the concentrations of the oligonucleotides used in this study, which is critical to the determination of steady state rate constants. We next measured the rate in the presence of saturating APE1 to evaluate the ability of APE1 to stimulate the dissociation of AAG on these different substrates (*8*).

Representative multiple-turnover data for the symmetric substrates are shown in Figure 4A, and the k_{cat} values are listed in Table 1. The k_{cat} values were very similar (~0.03 min^{-1}) for the substrates that were longer than 25 bp, whereas they increased rapidly as the substrate was shortened below 25 bp (Table 1). For the symmetric 17mer, the k_{cat} value increased by ~10-fold relative to that of the 25mer symmetric substrate. This demonstrates that AAG dissociates much more quickly from the shorter substrates in which there are fewer than 12 bp of flanking DNA. These shorter symmetric substrates were very efficiently stimulated by APE1, such that the multiple-turnover rate is essentially identical to the single-turnover rate of AAG-catalyzed Hx excision (Table 1). We define the efficiency of stimulation to be the ratio of the stimulated multiple-turnover rate constant divided by the single-turnover rate constant in the absence of APE1 (k_{cat}^{APE1}/k_{max}), and this value is ~1 for the 17- and 19mer symmetric substrates. To our surprise, the longer substrates were not as efficiently stimulated. Burst experiments confirmed the relative concentration of AAG and DNA, ruling out the trivial possibility that k_{cat} was incorrectly calculated (data not shown). Stimulated rates were independent of the concentration of APE1 from 2 to 10 μM, demonstrating that sufficient APE1 was present under our reaction conditions to saturate the stimulatory effect (see the Supporting Information). Apparently, the nonspecific flanking DNA provides a binding site for the displaced AAG and results in a slower rate of dissociation.

We next compared the rates for multiple-turnover excision of Hx from the asymmetric substrates in the presence and absence of APE1 (Figure 4B). In the absence of APE1, the k_{cat} values for the asymmetric 19 bp substrates are similar to that of the symmetric 19mer, indicating suboptimal binding of AAG to the abasic product in these shortened substrates (Table 1). Both substrates are stimulated to a similar extent by APE1 (7−10-fold stimulation), indicating the APE1 is able to displace AAG from either substrate. The substrate that was shortened on the downstream side is fully stimulated up to the rate of the single-turnover glycosylase reaction (efficiency of stimulation = 1). In contrast, the substrate that is shortened on the upstream side is not fully stimulated and has an efficiency of stimulation of only 0.3 (Table 1). At first glance, these data would seem to indicate that APE1 cannot displace AAG as efficiently if the upstream nonspecific DNA binding site is shortened. However, additional models must be considered, such as reduced binding affinity of APE1 for the 19u abasic site or end-fraying effects that might alter the nonspecific DNA binding of AAG.

The asymmetric substrates place the lesion close to the end of the duplex; therefore, we considered the possibility that the differences in the efficiency of stimulation for the 19u and 19d substrates were due to differential recognition by either AAG or APE1. We determined the relative k_{cat}/K_M values for AAG by directly competing these two substrates in the same reaction. The

Table 1: Kinetic Parameters for Excision of Hx by AAG in the Presence and Absence of APE1[a]

oligo name	*x*-fold stimulation[b]	k_{cat} (min^{-1}) without APE1[c]	k_{cat} (min^{-1}) with APE1[c]	k_{max} (min^{-1}) without APE1[d]	efficiency of stimulation[e]
		Central Lesion			
49mer	36	0.027 ± 0.003	0.97 ± 0.1	3.2 ± 0.6	0.3
35mer	57	0.028 ± 0.002	1.6 ± 0.1	3.9 ± 0.3	0.4
25mer[f]	66	0.036 ± 0.007	2.3 ± 0.3	2.8 ± 0.4	0.8
19mer[g]	20	0.10 ± 0.02	2.0 ± 0.5	2.2 ± 0.5	0.9
17mer[g]	8	0.23 ± 0.06	1.9 ± 0.2	1.8 ± 0.3	1.1
HP17PEG	25	0.088 ± 0.017	2.2 ± 0.3	2.4 ± 0.6	0.9
		5′ Lesion			
19u	10	0.059 ± 0.013	0.60 ± 0.07	2.4 ± 0.7	0.3
HP19u	52	0.032 ± 0.006	1.6 ± 0.4	3.1 ± 0.3	0.5
HP19uPEG	52	0.046 ± 0.008	2.4 ± 0.2	3.9 ± 0.3	0.6
		3′ Lesion			
19d	7	0.15 ± 0.03	1.1 ± 0.1	1.1 ± 0.2	1.0
HP19d	52	0.051 ± 0.005	2.5 ± 0.1	1.8 ± 0.5	1.4
21d	19	0.11 ± 0.02	2.2 ± 0.7	2.0 ± 0.4	1.1

[a]The rate constants for single-turnover and multiple-turnover excision of Hx were measured for full-length AAG under the standard low ionic strength conditions (see Materials and Methods). The DNA sequences are given in Figure 1. [b]The *x*-fold stimulation of AAG-catalyzed multiple turnovers by APE1 is calculated as the ratio of k_{cat} in the presence and absence of saturating APE1 [*x*-fold stimulation = (k_{cat} with APE1)/(k_{cat} without APE1)]. [c]Multiple-turnover excision of Hx was assessed with 1 μM substrate either in the presence or in the absence of 2 μM APE1. [d]The single-turnover rate constant was determined with a saturating concentration of AAG. [e]The efficiency of stimulation is given by the ratio of the APE1-stimulated k_{cat} value and the single-turnover rate constant (k_{cat}^{APE1}/k_{max}). [f]The steady state parameters for this substrate are very similar to the previously reported values (*8*). [g]Data from ref *8*.

results showed that AAG prefers the 19u substrate by a factor of ~3 over the 19d substrate (see the Supporting Information). This is consistent with the reduced single-turnover rate constant and increased rate of product dissociation for the 19d substrate (Table 1). We next determined the relative k_{cat}/K_M values for APE1-catalyzed strand nicking with these asymmetric oligonucleotides by mixing together the two abasic DNA products and following the APE1-catalyzed hydrolysis in the presence of Mg^{2+}. At low ionic strengths, identical k_{cat}/K_M values were obtained for 19u and 19d, consistent with a Briggs−Haldane mechanism (see the Supporting Information and ref *31*). Therefore, we increased the ionic strength to 140 mM to allow rapid equilibrium DNA binding by APE1. Under these conditions, a 3-fold higher k_{cat}/K_M was observed for the 19u relative to the 19d substrate (see the Supporting Information). Thus, APE1 and AAG both exhibit a similar preference for the 19u substrate. This rules out decreased binding affinity by APE1 as the cause of the low efficiency of APE1 stimulation on the 19u substrate.

We next considered the possibility that AAG might remain bound to the APE1·abasic DNA complex and does not immediately dissociate into solution. If this were true, then we would predict tighter binding of AAG to the 19u product than the 19d product when APE1 is also bound, because the stimulated rate is slower for the 19u substrate. Under initial rate conditions, the product complexes do not accumulate, and rebinding to product is not significant (*8*). However, if a multiple-turnover reaction is allowed to proceed to completion, then the product complex can compete for substrate binding. We followed AAG-catalyzed reactions with 19u and 19d asymmetric substrates and the 25mer symmetric substrate to completion in the presence of APE1 (Figure 5). The initial rates and the product inhibition are both different for these substrates, making it difficult to see that the 19d substrate shows a reduced level of product inhibition relative to the 19u and 25mer substrates. This is most easily visualized by replotting the data as a double-x plot that normalizes the initial rate portion of the reaction progress curves, allowing for a direct comparison of curvature due to product inhibition. Remarkably, the 19u and 25mer substrates show essentially identical product inhibition [note the curvature in the reaction progress curve at ~50% completion (Figure 5B)]. In contrast, the 19d substrate shows much less curvature, indicative of weakened product inhibition relative to that of the 25mer substrate (Figure 5C). These data could be simulated using a simple kinetic mechanism that takes into account substrate and product binding and the rate constant for multiple-turnover base excision (k_{cat}). These simulations revealed that the product inhibition for AAG glycosylase activity toward the 19d substrate is ~3-fold reduced relative to the product inhibition observed with the 19u and 25mer substrates (see the Supporting Information). These experiments confirm that AAG is more easily displaced from the 19d product than from the 19u product. This could indicate a stronger ability of APE1 to displace AAG from the upstream side but also requires that AAG preferentially bind downstream of APE1. Thus, a putative protein−protein interaction would be destabilizing with respect to AAG binding to the abasic site, but stabilizing with respect to AAG binding to nonspecific DNA. We think it is more likely that these differences in the asymmetric substrates are due to different end fraying effects for the two substrates, as discussed below. Regardless of the source of the different kinetic behavior for asymmetric substrates of opposite polarity, it is important to recognize that APE1 is able to efficiently stimulate the dissociation of AAG even though the AAG footprint extends to the ends of the DNA.

Use of Hairpin Structures To Minimize End Fraying Effects. The increased k_{cat} values for the shortened substrates, especially the 17mer symmetric substrate and the 19d asymmetric substrate, suggest that end fraying might be responsible for the increased rate of dissociation of AAG from these abasic DNA products. This is because the AAG−DNA contacts identified in the crystal structure do not extend beyond 6 bp from the

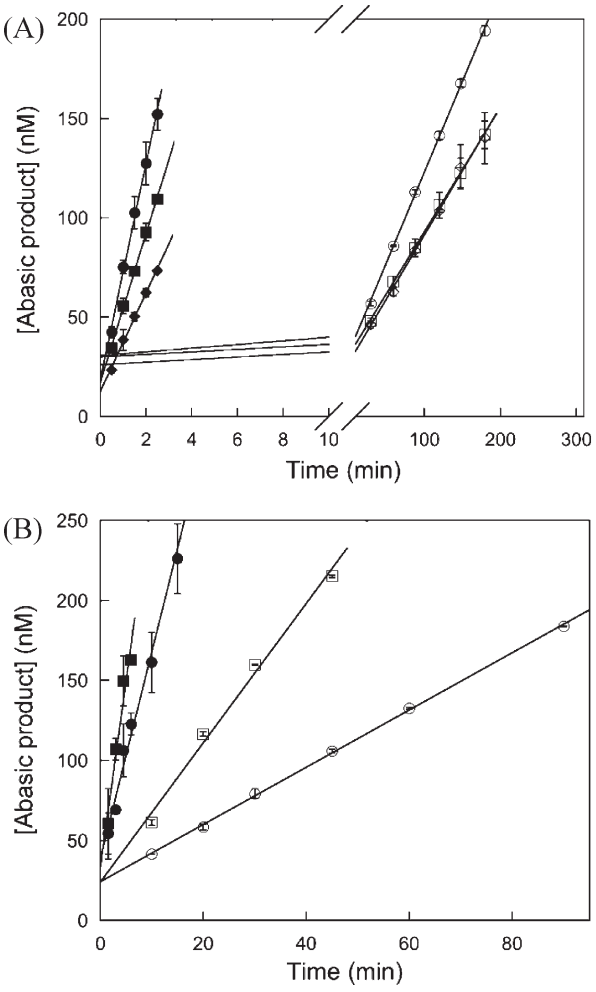

FIGURE 4: Multiple-turnover excision of Hx by AAG and the stimulation by APE1. Representative data for select substrates are shown. Multiple-turnover reactions were performed in duplicate or triplicate with 25 nM AAG and the indicated substrate at 1 μM in the presence (filled symbols) or absence (empty symbols) of 2 μM APE1. (A) The results for the symmetric 25mer (○), 35mer (□), and 49mer (◇) substrates are compared. (B) Comparison of the results for the asymmetric substrates in which either the upstream (19u, ○) or downstream (19d, □) flanking DNA was shortened.

lesion (*29*). Therefore, we prepared a 17 bp duplex that was joined by a polyethylene glycol (PEG) linker to form a hairpin structure (*32*), reasoning that the hairpin would decrease the level of fraying of this end (Figure 1). This hairpin resulted in a 2.6-fold decrease in k_{cat}, reflecting tighter binding to the less flexible hairpin relative to a blunt end. In contrast, the single-turnover rate constant was essentially unchanged [increased by 1.3-fold (Table 1)]. Because of the greater difference between base excision and product dissociation rates, the *x*-fold stimulation of AAG by APE1 is increased 3-fold for the hairpin even though the efficiency of stimulation is ~1 for both 17mer substrates (Table 1).

To evaluate the effects of end fraying on the asymmetric 19mer substrates, we synthesized analogous substrates in which the shorter flanking arms were connected by either a PEG linker or a GAAA tetraloop hairpin. We measured single-turnover and multiple-turnover glycosylase activity, and the results are summarized in Table 1. When the upstream flanking region was shortened (5′ lesion position), both the PEG and GAAA tetraloop exhibited very similar kinetic parameters. This suggests that both hairpins decrease the level of end fraying and stabilize the duplex, allowing more favorable DNA binding contacts with

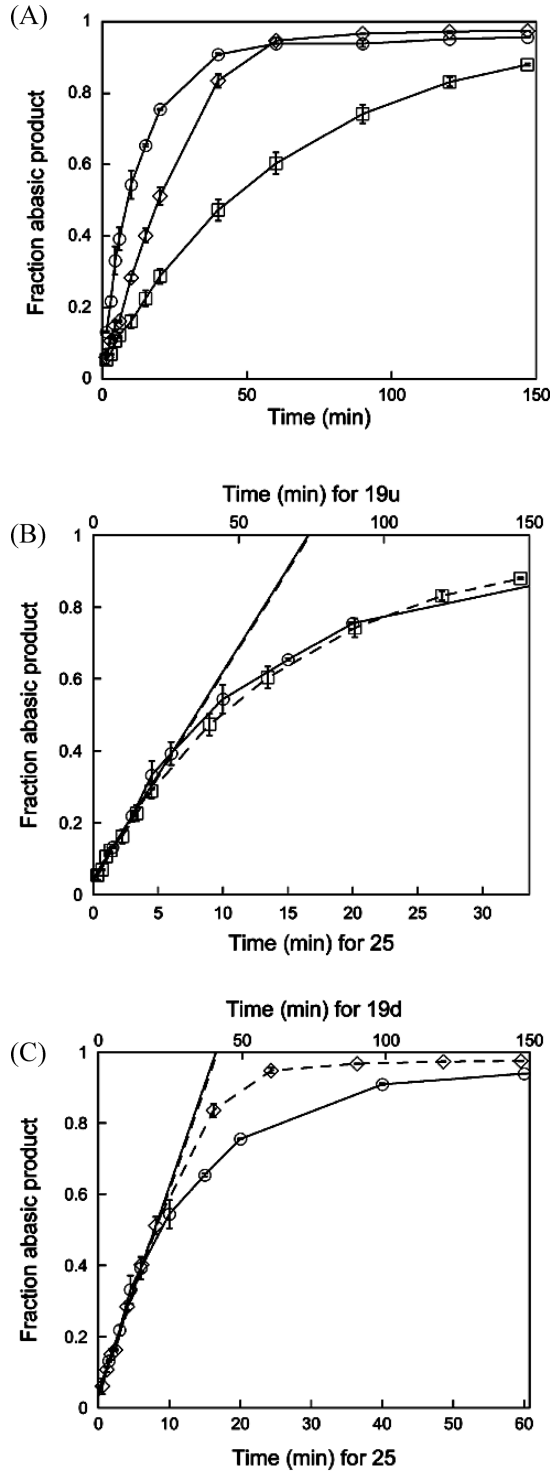

FIGURE 5: Differential product inhibition in APE1-stimulated AAG multiple-turnover reactions. (A) Multiple-turnover reactions for the 25mer (○), 19u (□), and 19d (◇) substrates containing both AAG and APE1 were set up as described in the legend of Figure 4, but time points were taken up to ≥85% completion. The ability of AAG to rebind to the APE1·abasic DNA complex can be inferred from the curvature in the reaction progress curve. Double-x plots were generated from the same data to facilitate the direct comparison of product inhibition. Initial rates were calculated from the first 20% of the reaction (straight line), and the time scales were adjusted so that the initial rates for the two substrates overlap. (B) The 25mer (○) and 19u (□) substrates exhibit indistinguishable product inhibition. (C) The 25mer (○) substrate shows greater product inhibition than the 19d (◇) substrate. These data were further analyzed by global simulations using Berkeley Madonna, which revealed ~3-fold reduced product inhibition for the 19d substrate relative to the 19u and 25mer substrates (see the Supporting Information).

AAG. For the hairpin substrates, the rate of dissociation of AAG from its abasic DNA product was slowed and the APE1-stimulated rate was increased to provide an ~5-fold increase in the stimulation (Table 1). The shortening of the downstream DNA (3′ lesion position) had weaker effects on AAG activity, but a hairpin on this end (HP19d) also provided more stable binding by AAG. The 3-fold decrease in k_{cat} demonstrates that the AAG binding affinity is increased. This resulted in a 7-fold increase in the level of stimulation by APE1 (Table 1).

An Unrelated Enzyme Can Also Displace AAG from Its Abasic DNA Product. The data provided above are consistent with the model in which AAG transiently diffuses from the abasic site along the DNA. This would provide an opportunity for APE1 to capture the abasic site and prevent rebinding of AAG. This model predicts that other enzymes that bind to abasic sites would be able to compete and thereby increase the macroscopic rate of dissociation from the DNA. We tested this hypothesis with a bifunctional bacterial DNA glycosylase, *E. coli* EndoIII, because this enzyme can bind to and hydrolyze abasic sites via a lyase mechanism. *E. coli* does not have a structural homologue of AAG; therefore, it is unlikely that the *E. coli* EndoIII protein is capable of specific protein−protein interactions with the human AAG protein. In addition to its AP lyase activity, EndoIII is known to recognize oxidized pyrimidine lesions (*33*). We tested whether EndoIII could recognize an I·T lesion and found extremely low glycosylase activity toward this substrate (see the Supporting Information). Therefore, an increase in multiple-turnover glycosylase activity of AAG would be indicative of stimulation by binding of EndoIII to the abasic site.

Under multiple-turnover conditions for which dissociation from the abasic product limits the rate of the AAG reaction, we observed robust stimulation by EndoIII (Figure 6). The stimulation by EndoIII reaches almost the same rates that were observed for APE1, but the concentration dependence shows that it does not compete for the abasic site as well as APE1. This is consistent with the known affinities of these proteins for an abasic site. Whereas APE1 binds with picomolar to nanomolar affinity (*24*, *34*), EndoIII is reported to bind with micromolar affinity (*35*). These data suggest that AAG transiently exposes the abasic site and protein−protein interactions are not necessary for increasing the rate of AAG dissociation.

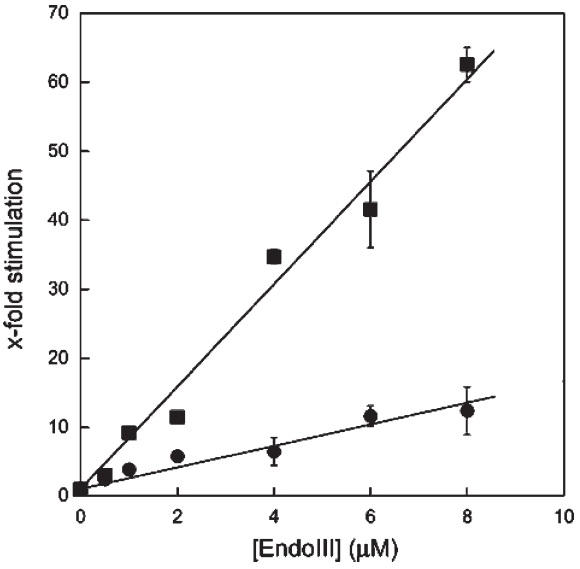

FIGURE 6: Stimulation of AAG by *E. coli* EndoIII. Multiple-turnover (k_{cat}) AAG glycosylase activity on the 17mer (●) and 25mer (■) substrates was measured in the presence of different concentrations of EndoIII. The stimulation (*x*-fold) was calculated from the ratio of k_{cat} in the presence of EndoIII to that measured for AAG alone. The concentration dependence was roughly linear up to the highest concentration of EndoIII achieved (8 μM). The extent of stimulation by 8 μM EndoIII for both substrates is essentially the same as that observed for stimulation by APE1 under these conditions (Table 1). EndoIII exhibited extremely slow glycosylase activity toward inosine under these conditions but did not contribute to the measured rate of Hx excision when both EndoIII and AAG were present (see the Supporting Information).

DISCUSSION

Previous studies of the coordination of the first two steps of base excision repair for several different glycosylases found that APE1 increases the rate of dissociation of the glycosylase from its abasic DNA product (*2*, *6*−*8*). This could result from direct protein−protein interaction between the glycosylase and APE1. However, APE1 is known to bind nonspecifically to DNA and has been reported to use these nonspecific DNA binding interactions to locate sites of damage in the absence of other repair proteins (*15*). Therefore, we have also considered the possibility that APE1 and the glycosylase switch places without either protein dissociating into solution. These two general mechanisms might be distinguished by examining the ability of APE1 to stimulate multiple-turnover glycosylase activity with asymmetric substrates (*7*). If APE1 were to make a specific interaction with AAG, then it is expected that APE1 would be positioned on one side or the other and that removing this flanking region would interfere with the ability of APE1 to stimulate the rate of AAG dissociation. If only nonspecific DNA binding interactions are required, then APE1 would be expected to stimulate the glycosylase from either flanking region.

Contributions of the Upstream (*5′ flanking*) *Region*. Crystal structures of AAG bound to DNA reveal protein−DNA contacts 5 bp upstream (5′ to the lesion) on the opposing strand [Figure 7 (*36*)]. Therefore, we shortened this region to 6 bp, with the expectation that this would provide a minimal binding site for AAG without leaving room for APE1 to bind. We found that this asymmetric substrate (19u) is a good substrate for AAG, with a single-turnover rate constant essentially identical to that of the longer 25mer substrate (Figure 8). The rate of dissociation from the 19u abasic DNA product is increased by ~2-fold. This modest decrease in the stability of the AAG·abasic DNA complex was restored when the end was stabilized with either a PEG linker or a GAAA tetraloop. Surprisingly, the APE1 stimulation is dramatically decreased for the 19u substrate. This could indicate that the upstream DNA is required for APE1 binding and that the reduced binding site results in less efficient stimulation. Similar logic has been previously employed in the study of the APE1 stimulation of OGG1, in which the same polarity was observed (*7*). However, the hairpins of the same length rescued this defect and allowed for more efficient stimulation (Figure 8). This suggests that there are complex effects due to end fraying that are relieved by hairpin formation. The results from the hairpin substrates are more informative, and they demonstrate that as little as 6 bp of upstream flanking DNA is sufficient for APE1 stimulation of AAG. This result demonstrates that APE1 does not have to interact with the lesion-containing strand upstream from AAG to stimulate its release.

Contributions of the Downstream (*3′ flanking*) *Region*. Analogous experiments were used to evaluate the effect of shortening the DNA downstream of the lesion (Figure 9). Shortening this

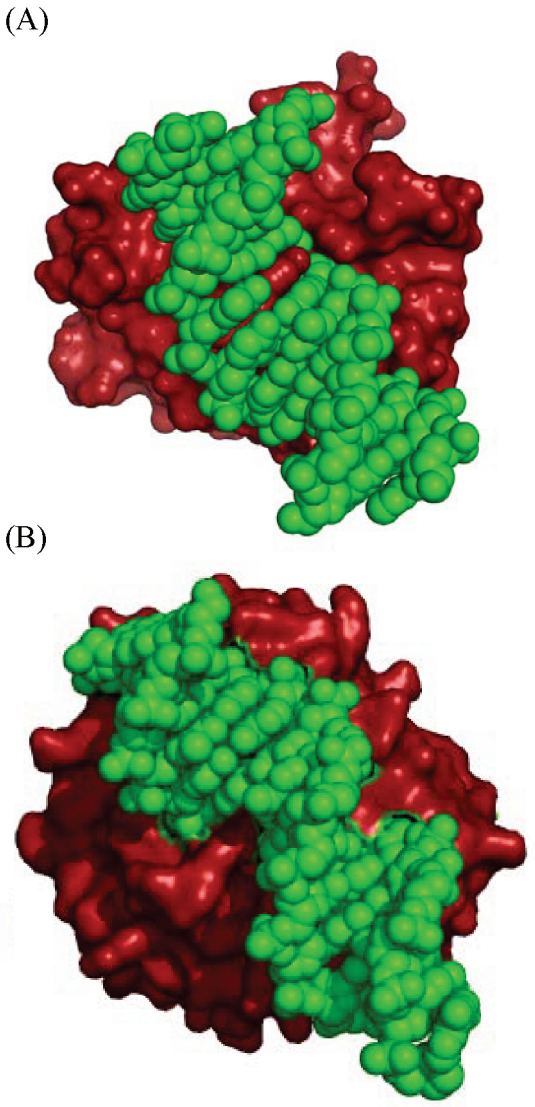

FIGURE 7: Structures of AAG and APE1. Space-filling representations of (A) AAG bound to a 13mer εA-DNA [PDB entry 1EWN (*36*)] and (B) APE1 bound to a 15mer abasic DNA [PDB entry 1DEW (*39*)]. Protein surfaces are colored red, and DNA is colored green. Both interact predominantly with one surface of the DNA. Therefore, it can be envisioned that both AAG and APE1 might simultaneously bind by interacting with opposing surfaces.

region to 6 bp resulted in a slight ~2-fold decrease in the maximal single-turnover rate constant for AAG, relative to the symmetric substrate that has a 12 bp downstream region. This suggests that binding interactions beyond 6 bp make a modest contribution to the excision of Hx. This is surprising, because no contacts were observed in the crystal structure in this region. However, the protein that was crystallized lacked the first ~79 amino acids, and we have used the full-length protein in these studies. Stabilization of the downstream DNA end with a hairpin or by extension of the duplex to 8 bp partially restored the full glycosylase activity (Figure 9A). These asymmetric substrates with a shortened downstream region exhibited significantly faster rates of dissociation from the abasic DNA products, consistent with important AAG−DNA contacts in this flanking region (Figure 9B). These destabilizing effects were likely influenced by end fraying, because the hairpin substrate showed a rate of product dissociation similar to that of the symmetric 25mer. The 19d and 21d substrates show greatly reduced stimulation by APE1, but this is simply due to the

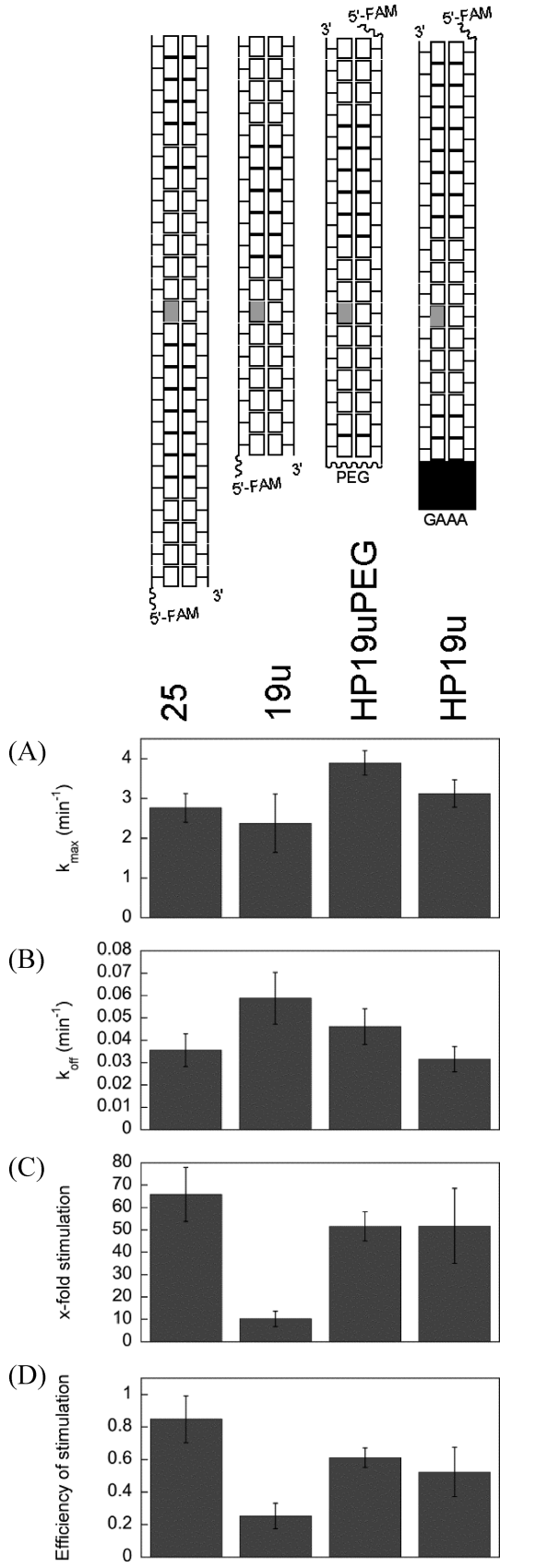

FIGURE 8: Evaluation of AAG activity and stimulation by APE1 near the 5′ (upstream) end. The values of k_{max} (A) and k_{off} (B) were measured in the absence of APE1, and the *x*-fold stimulation (C) and efficiency of stimulation (D) were determined with a saturating concentration of APE1 (Table 1).

decreased glycosylase activity and the increased rate of dissociation of AAG in the absence of APE1 (Figure 9C and Table 1).

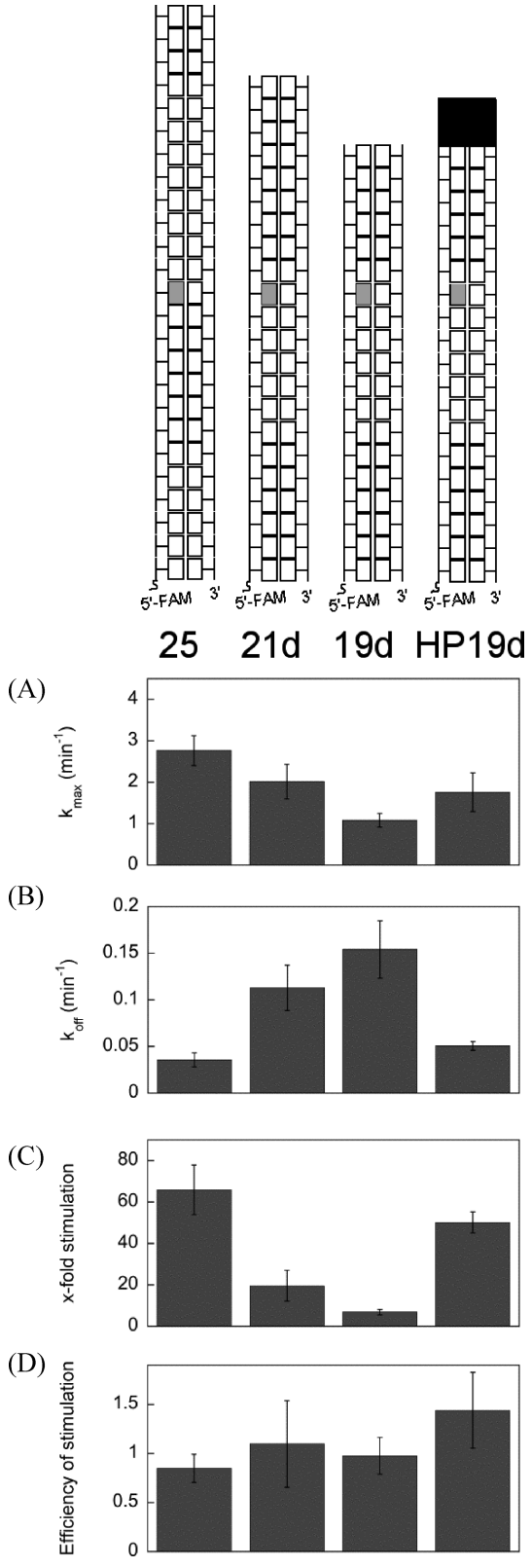

FIGURE 9: Evaluation of AAG activity and stimulation by APE1 near the 3′ (downstream) end. The values of k_{max} (A) and k_{off} (B) were measured in the absence of APE1, and the *x*-fold stimulation (C) and efficiency of stimulation (D) were determined with a saturating concentration of APE1 (Table 1).

When the efficiency of stimulation is calculated, it is apparent that APE1 fully stimulates AAG turnover on these substrates so that the overall rate of reaction is limited by base excision and not product dissociation. Thus, this series of substrates provided compelling evidence that APE1 does not bind to the lesion-containing strand downstream of AAG. Because both upstream and downstream flanking regions can be shortened to the point where AAG activity is affected and yet APE1 efficiently stimulates, we favor the model in which APE1 uses nonspecific DNA binding interactions to displace AAG. However, these experiments do not address the possibility that a protein−protein interaction might be made across the DNA duplex.

Effect of Flanking DNA Length on the Activity of AAG and the Stimulation by APE1. We obtained additional insight into the mechanism of AAG displacement by APE1 by examining the multiple-turnover reaction of AAG on oligonucleotides containing a central lesion and different lengths of flanking DNA. Even the shortest of these substrates (17 bp) is a good substrate for AAG (Figure 10A). However, the shorter duplexes do result in destabilization of the AAG·abasic DNA complex, because the rate of dissociation increased by ~10-fold as the length was decreased from 35 to 17 bp (Figure 10B). As discussed above, fraying of the DNA ends is likely to account for the decreased affinity (increased dissociation rate constant) of the shorter substrates. We tested a 17mer symmetric substrate in which the downstream end was stabilized by a PEG hairpin, and this resulted in ~3-fold stabilization of the AAG·abasic DNA complex [HP17PEG (Table 1)]. The single-turnover and multiple-turnover glycosylase activity of AAG in the absence of APE1 is consistent with the data collected for the asymmetric substrates and can easily be explained by the DNA binding interactions observed in the AAG·DNA crystal structure (Figure 7). However, the stimulation of AAG by APE1 yielded a surprise.

The overall level of stimulation by APE1 increases as the DNA length is increased from 17 to 25 bp (Figure 10C). This can be explained by the more stable binding of AAG to longer substrates, and efficient binding of APE1 to substrates as short as 17 bp. For all of these substrates, the APE1-stimulated rate is independent of the concentration of APE1, suggesting that APE1 is saturating and able to bind to the AAG·DNA complex. The 35- and 49mer substrates show a slight decrease in the *x*-fold stimulation by APE1. This decrease is even more apparent when the efficiency of stimulation is calculated (Figure 10D). Clearly, the ability of APE1 to stimulate AAG decreases as the DNA length is increased. This decrease in the efficiency of stimulation is due mostly to a decrease in the APE1-stimulated rate of AAG, with only modest changes in k_{off} and k_{max} in the absence of APE1 (Figure 10). The simplest model for explaining this behavior is that APE1 does not directly displace AAG into solution but rather displaces it along the DNA. The stimulated k_{cat} value of ~1 min^{-1} for AAG turnover on the 49mer substrate in the presence of APE1 is likely to reflect the rate of dissociation of AAG from undamaged DNA. Stopped-flow binding experiments with AAG binding to εA-DNA yielded a similar value of ~0.5 min^{-1} for the dissociation of AAG from nonspecific DNA under slightly different conditions (*28*). The increased value of k_{cat} for the shorter substrates is likely due to unstable binding of AAG in the presence of bound APE1 which occupies a considerable fraction of the available DNA surface (*8*).

Implications for the Mechanism of APE1 Stimulation of AAG. Our working model for the coordination of the first two steps of the BER pathway catalyzed by AAG and APE1 is summarized in Figure 11. Recent studies that explored the processivity of AAG demonstrated that AAG uses nonspecific DNA binding interactions to search DNA for sites of damage (*14*, *37*). Although AAG binds tightly to the abasic site, it does with some

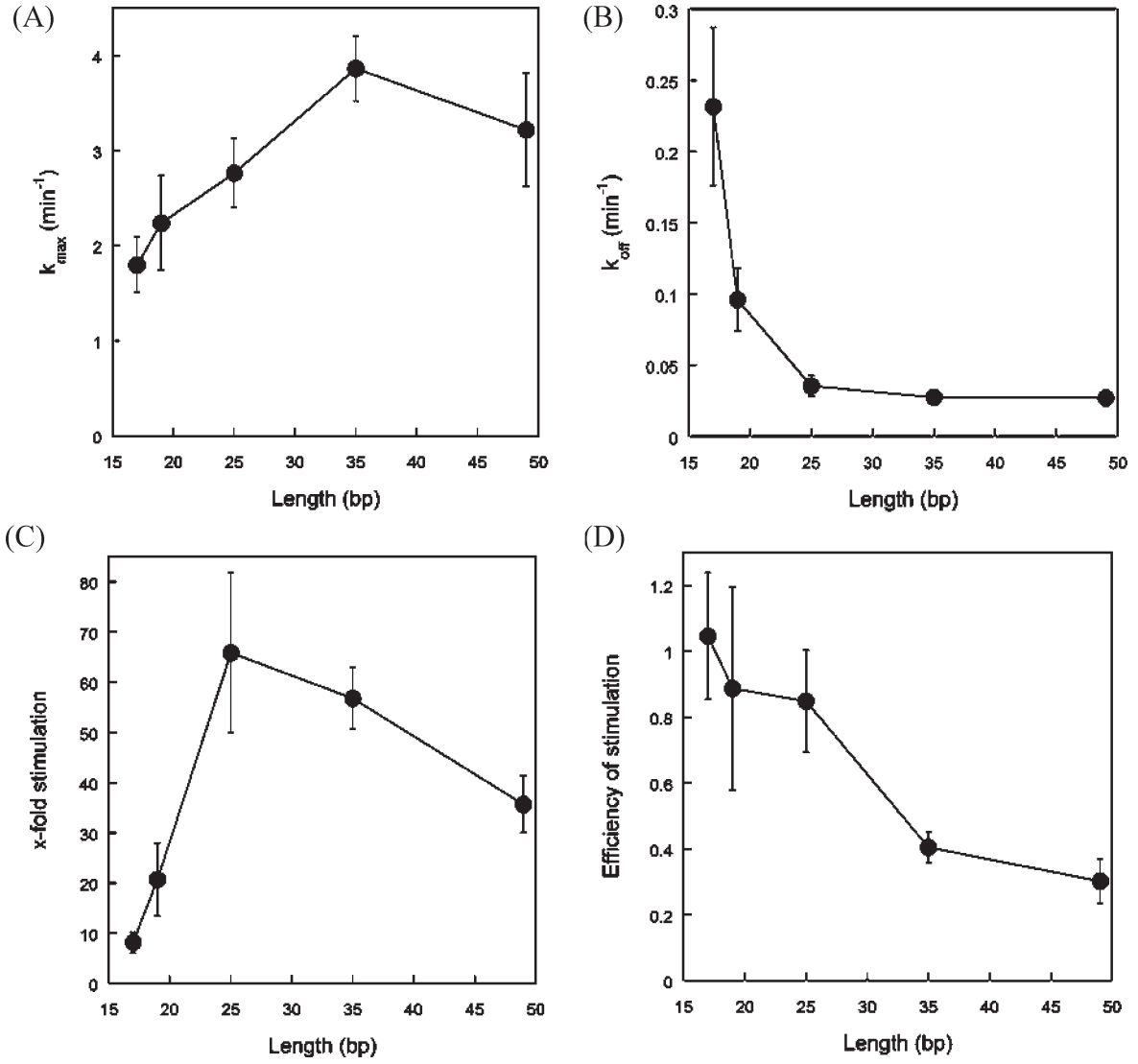

FIGURE 10: Evaluation of AAG activity and stimulation by APE1 on symmetrical oligonucleotide substrates. (A) Single-turnover (k_{max}) and (B) multiple-turnover ($k_{cat} = k_{off}$) rate constants are plotted for AAG-catalyzed excision of Hx in the absence of APE1. The APE1 stimulation of AAG on these same substrates is plotted as either the *x*-fold stimulation (C) or the efficiency of stimulation (D). The values are taken from Table 1, and the error bars indicate the standard deviation. The points are connected to guide the eye.

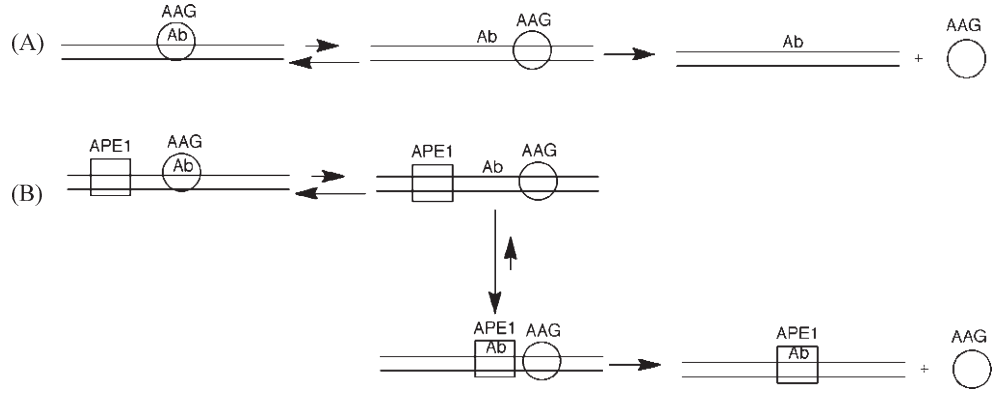

FIGURE 11: Mechanism for APE1 stimulation of AAG dissociation from the abasic DNA product. (A) In the absence of APE1, AAG (circle) is in rapid equilibrium between being bound with high affinity to the abasic site and being bound with lower affinity to adjacent nonspecific sites. Occasionally, AAG dissociates from the nonspecific DNA but usually returns to the abasic site without dissociating into solution. (B) APE1 (square) is able to capture the transiently exposed abasic site and prevent rebinding by AAG. This leads to an increase in the observed rate of dissociation of AAG into solution.

frequency leave the site and diffuses along the DNA (Figure 11A). Most often, AAG returns to the abasic site without dissociating into solution. Therefore, in the absence of APE1, the abasic site is afforded some protection by being bound to AAG. However, if APE1 is present, it can capture the transiently exposed abasic site (Figure 11B). These transient excursions are frequent enough

that the dissociation of AAG is not the rate-limiting step. We have shown that both APE1 and *E. coli* EndoIII are able to capture the abasic site as fast as it is formed by AAG. This model does not require specific interactions between proteins, as long as both proteins can bind DNA nonspecifically and diffuse along it. The binding affinity, and thus the binding lifetime, will favor the complex that is most stable. It has previously been suggested that the high affinity of APE1 for its abasic substrate and the high affinity of pol β for the nicked 5′-dRP intermediate provide a mechanism for ensuring the transition of the BER intermediate from APE1 to pol β (*24*). Given that the intermediates in the BER pathway need to directly make a transition from one active site to the next, a dynamic mechanism of transitions between specific and nonspecific DNA sites would allow for the sampling and selection of thermodynamically favored complexes that could be further processed along the BER pathway.

The structural information places strong constraints on the biochemical observations that are described above. Although we cannot rule out the possibility that specific protein−protein interactions exist between AAG and APE1, the considerations discussed above suggest that effective coordination could be achieved even in the absence of direct interactions. If no specific protein−protein contacts are made, the two proteins nevertheless come into proximity on the very short oligonucleotides that we have studied, because the footprints for binding of AAG and APE1 are both ~8 bp (Figure 7). Therefore, it is unlikely that both bind to the same face of the DNA on a duplex with as little as 8 bp of flanking DNA, as is present in the 17mer symmetric substrate. If APE1 is initially bound on the opposing strand, then it would need to switch strands to be able to bind to the abasic site. AAG and uracil DNA glycosylase have both been shown to rapidly sample both strands while they are bound, so it is possible that this is a general property of DNA binding proteins (*37*, *38*).

The concept that nonspecific DNA binding interactions facilitate the exchange of BER enzymes during the course of DNA repair is attractive, because it can explain why a single AP endonuclease is able to accept abasic DNA intermediates from any of 11 different glycosylases that come from different structural families and do not appear to share any common interaction surfaces. Nonspecific DNA binding interactions appear to be critical not only for the initial recognition of DNA damage but also for the coordination of the multistep BER pathway.

ACKNOWLEDGMENT

We thank members of the O'Brien lab for critical reading of the manuscript and Patricia Pellicena and Matt Young for the gift of the pET-based expression vector encoding His-tagged SUMO.

SUPPORTING INFORMATION AVAILABLE

Representative data are presented in which the AAG concentration is varied under single-turnover conditions, the APE1 concentration is varied under single- and multiple-turnover conditions, APE1 catalyzes cleavage of a PEG linker, and EndoIII catalyzes a slow excision of Hx. The relative k_{cat}/K_M values for recognition of the 19d and 19u substrates by AAG and APE1 are determined by competition experiments, and kinetic simulations are used to characterize the differential product inhibition with the different substrates. This material is available free of charge via the Internet at http://pubs.acs.org.

REFERENCES

1. Porello, S. L., Leyes, A. E., and David, S. S. (1998) Single-turnover and pre-steady-state kinetics of the reaction of the adenine glycosylase MutY with mismatch-containing DNA substrates. *Biochemistry 37*, 14756–14764.
2. Waters, T. R., Gallinari, P., Jiricny, J., and Swann, P. F. (1999) Human thymine DNA glycosylase binds to apurinic sites in DNA but is displaced by human apurinic endonuclease 1. *J. Biol. Chem. 274*, 67–74.
3. Petronzelli, F., Riccio, A., Markham, G. D., Seeholzer, S. H., Stoerker, J., Genuardi, M., Yeung, A. T., Matsumoto, Y., and Bellacosa, A. (2000) Biphasic kinetics of the human DNA repair protein MED1 (MBD4), a mismatch-specific DNA N-glycosylase. *J. Biol. Chem. 275*, 32422–32429.
4. Maher, R. L., Vallur, A. C., Feller, J. A., and Bloom, L. B. (2007) Slow base excision by human alkyladenine DNA glycosylase limits the rate of formation of AP sites and AP endonuclease 1 does not stimulate base excision. *DNA Repair 6*, 71–81.
5. Hill, J. W., Hazra, T. K., Izumi, T., and Mitra, S. (2001) Stimulation of human 8-oxoguanine-DNA glycosylase by AP-endonuclease: Potential coordination of the initial steps in base excision repair. *Nucleic Acids Res. 29*, 430–438.
6. Fitzgerald, M. E., and Drohat, A. C. (2008) Coordinating the initial steps of base excision repair. Apurinic/apyrimidinic endonuclease 1 actively stimulates thymine DNA glycosylase by disrupting the product complex. *J. Biol. Chem. 283*, 32680–32690.
7. Sidorenko, V. S., Nevinsky, G. A., and Zharkov, D. O. (2007) Mechanism of interaction between human 8-oxoguanine-DNA glycosylase and AP endonuclease. *DNA Repair 6*, 317–328.
8. Baldwin, M. R., and O'Brien, P. J. (2009) Human AP Endonuclease I Stimulates Multiple-Turnover Base Excision by Alkyladenine DNA Glycosylase. *Biochemistry 48*, 6022–6033.
9. O'Brien, P. J., and Ellenberger, T. (2004) Dissecting the broad substrate specificity of human 3-methyladenine-DNA glycosylase. *J. Biol. Chem. 279*, 9750–9757.
10. Hitchcock, T. M., Dong, L., Connor, E. E., Meira, L. B., Samson, L. D., Wyatt, M. D., and Cao, W. (2004) Oxanine DNA glycosylase activity from mammalian alkyladenine glycosylase. *J. Biol. Chem. 279*, 38177–38183.
11. Karran, P., and Lindahl, T. (1980) Hypoxanthine in deoxyribonucleic acid: Generation by heat-induced hydrolysis of adenine residues and release in free form by a deoxyribonucleic acid glycosylase from calf thymus. *Biochemistry 19*, 6005–6011.
12. Saparbaev, M., and Laval, J. (1994) Excision of hypoxanthine from DNA containing dIMP residues by the *Escherichia coli*, yeast, rat, and human alkylpurine DNA glycosylases. *Proc. Natl. Acad. Sci. U.S.A. 91*, 5873–5877.
13. Miao, F., Bouziane, M., Dammann, R., Masutani, C., Hanaoka, F., Pfeifer, G., and O'Connor, T. R. (2000) 3-Methyladenine-DNA glycosylase (MPG protein) interacts with human RAD23 proteins. *J. Biol. Chem. 275*, 28433–28438.
14. Hedglin, M., and O'Brien, P. J. (2008) Human alkyladenine DNA glycosylase employs a processive search for DNA damage. *Biochemistry 47*, 11434–11445.
15. Carey, D. C., and Strauss, P. R. (1999) Human apurinic/apyrimidinic endonuclease is processive. *Biochemistry 38*, 16553–16560.
16. O'Brien, P. J., and Ellenberger, T. (2003) Human alkyladenine DNA glycosylase uses acid-base catalysis for selective excision of damaged purines. *Biochemistry 42*, 12418–12429.
17. Kelley, M. R., and Parsons, S. H. (2001) Redox regulation of the DNA repair function of the human AP endonuclease Ape1/ref-1. *Antioxid. Redox Signaling 3*, 671–683.
18. Erzberger, J. P., and Wilson, D. M., III (1999) The role of Mg^{2+} and specific amino acid residues in the catalytic reaction of the major human abasic endonuclease: New insights from EDTA-resistant incision of acyclic abasic site analogs and site-directed mutagenesis. *J. Mol. Biol. 290*, 447–457.
19. Gros, L., Ishchenko, A. A., Ide, H., Elder, R. H., and Saparbaev, M. K. (2004) The major human AP endonuclease (Ape1) is involved in the nucleotide incision repair pathway. *Nucleic Acids Res. 32*, 73–81.
20. Ishchenko, A. A., Ide, H., Ramotar, D., Nevinsky, G., and Saparbaev, M. (2004) α-Anomeric deoxynucleotides, anoxic products of ionizing radiation, are substrates for the endonuclease IV-type AP endonucleases. *Biochemistry 43*, 15210–15216.
21. Dizdaroglu, M., Laval, J., and Boiteux, S. (1993) Substrate specificity of the *Escherichia coli* endonuclease III: Excision of thymine- and cytosine-derived lesions in DNA produced by radiation-generated free radicals. *Biochemistry 32*, 12105–12111.

22. Katafuchi, A., Nakano, T., Masaoka, A., Terato, H., Iwai, S., Hanaoka, F., and Ide, H. (2004) Differential specificity of human and *Escherichia coli* endonuclease III and VIII homologues for oxidative base lesions. *J. Biol. Chem. 279*, 14464–14471.
23. Fersht, A. (1999) Structure and Mechanism in Protein Science, 2nd ed., pp 16−17, W. H. Freeman, New York.
24. Liu, Y., Prasad, R., Beard, W. A., Kedar, P. S., Hou, E. W., Shock, D. D., and Wilson, S. H. (2007) Coordination of steps in single-nucleotide base excision repair mediated by apurinic/apyrimidinic endonuclease 1 and DNA polymerase β. *J. Biol. Chem. 282*, 13532–13541.
25. Masuda, Y., Bennett, R. A., and Demple, B. (1998) Rapid dissociation of human apurinic endonuclease (Ape1) from incised DNA induced by magnesium. *J. Biol. Chem. 273*, 30360–30365.
26. Wyatt, M. D., and Samson, L. D. (2000) Influence of DNA structure on hypoxanthine and 1,N(6)-ethenoadenine removal by murine 3-methyladenine DNA glycosylase. *Carcinogenesis 21*, 901–908.
27. Vallur, A. C., Maher, R. L., and Bloom, L. B. (2005) The efficiency of hypoxanthine excision by alkyladenine DNA glycosylase is altered by changes in nearest neighbor bases. *DNA Repair 4*, 1088–1098.
28. Wolfe, A. E., and O'Brien, P. J. (2009) Kinetic mechanism for the flipping and excision of 1,N(6)-ethenoadenine by human alkyladenine DNA glycosylase. *Biochemistry 48*, 11357–11369.
29. Lau, A. Y., Scharer, O. D., Samson, L., Verdine, G. L., and Ellenberger, T. (1998) Crystal structure of a human alkylbase-DNA repair enzyme complexed to DNA: Mechanisms for nucleotide flipping and base excision. *Cell 95*, 249–258.
30. Lyons, D. M., and O'Brien, P. J. (2009) Efficient recognition of an unpaired lesion by a DNA repair glycosylase. *J. Am. Chem. Soc. 131*, 17742–17743.
31. Strauss, P. R., Beard, W. A., Patterson, T. A., and Wilson, S. H. (1997) Substrate binding by human apurinic/apyrimidinic endonuclease indicates a Briggs-Haldane mechanism. *J. Biol. Chem. 272*, 1302–1307.
32. Ng, P. S., and Bergstrom, D. E. (2004) Protein-DNA footprinting by endcapped duplex oligodeoxyribonucleotides. *Nucleic Acids Res. 32*, e107.
33. Boorstein, R. J., Hilbert, T. P., Cunningham, R. P., and Teebor, G. W. (1990) Formation and stability of repairable pyrimidine photohydrates in DNA. *Biochemistry 29*, 10455–10460.
34. Maher, R. L., and Bloom, L. B. (2007) Pre-steady-state kinetic characterization of the AP endonuclease activity of human AP endonuclease 1. *J. Biol. Chem. 282*, 30577–30585.
35. O'Handley, S., Scholes, C. P., and Cunningham, R. P. (1995) Endonuclease III interactions with DNA substrates. 1. Binding and footprinting studies with oligonucleotides containing a reduced apyrimidinic site. *Biochemistry 34*, 2528–2536.
36. Lau, A. Y., Wyatt, M. D., Glassner, B. J., Samson, L. D., and Ellenberger, T. (2000) Molecular basis for discriminating between normal and damaged bases by the human alkyladenine glycosylase, AAG. *Proc. Natl. Acad. Sci. U.S.A. 97*, 13573–13578.
37. Hedglin, M., and O'Brien, P. J. (2010) Hopping enables a DNA repair glycosylase to search both strands and bypass a bound protein. *ACS Chem. Biol. 5*, 427–436.
38. Porecha, R. H., and Stivers, J. T. (2008) Uracil DNA glycosylase uses DNA hopping and short-range sliding to trap extrahelical uracils. *Proc. Natl. Acad. Sci. U.S.A. 105*, 10791–10796.
39. Mol, C. D., Izumi, T., Mitra, S., and Tainer, J. A. (2000) DNA-bound structures and mutants reveal abasic DNA binding by APE1 and DNA repair coordination [corrected]. *Nature 403*, 451–456.